Rotary Cross Spectral Analysis of Low Frequency Currents With Co-located Wind Measurements in the Southern Monterey Bay

ENS William C. Blodgett, Jr.
22MAR02
OC3570 - Operational Oceanography

TABLE OF CONTENTS

INTRODUCTION

The Monterey Inner Shelf Observatory (MISO) is part of an on-going program focused on littoral oceanographic observation and modeling at the Naval Postgraduate School, Monterey, CA. MISO, a component of the Rapid Environmental Assessment Laboratory (REAL), consists of an underwater frame supporting approximately five instruments: a Broadband Acoustic Doppler Current Profiler (BADCP), Paro-scientific pressure sensor, Scanning acoustic altimeter, Under-water video camera and laser light, and Bistatic Coherent Doppler Velocity and Sediment Profiler (BCDVSP).

The MISO frame is located 600 m off the Del Monte Beach at the southern end of the Monterey Bay (Figure 1). MISO, which is mounted on the seafloor 12m below the surface, is connected to a shore terminus by a fiber optic cable. A meteorological station in the sand dunes inshore augments the data collected underwater by measuring 10m height wind speed and direction, air temperature and dew point, short and long wave incident radiation, barometric pressure, and rain fall rates. Figure 2 illustrates the MISO and meteorological station's configuration.

MISO began collecting data on July 26, 1999, and the meteorological station began on April 28, 2000. Although the data set is not complete (due to instrument malfunction, failure, or maintenance), a large portion of continuously sampled data is available for study (Figure 3). The focus of this study will be to examine both the wind meteorological and ocean current data sets. Using complex rotary cross spectra, this study will determine the coupling of low frequency currents at two specific heights in the water column with co-located winds in the southern Monterey Bay. A comparison between the near-surface and near-bottom horizontal current velocities will demonstrate the degree of wind coupling throughout the water column.

EXPERIMENT

Data Acquisition

The Broadband Acoustic Doppler Current Profiler (BADCP) obtained the horizontal current velocities at the MISO site. In-situ measurements were transmitted through the fiber-optic cable and recorded to two output files at the shore terminus. The first output file contained the majority of the raw data: four beams of velocity data and their corresponding correlation magnitudes and echo intensities. The second file contained a record of BADCP profile characteristics for each ensemble average (i.e. date and time acquired and processed, pressure, sound speed, temperature, etc.). The BADCP sampled the water column in fractions of a second. Bad horizontal velocity measurements were flagged for easy identification prior to storage.

The BADCP measures the current velocity throughout the entire water column. In this experiment, only two specific depths were desired: one near the surface, and one near the sea floor. Velocities from the second bin (~3m off the bottom, or z≈9m) and tenth bin (~8m off the bottom, or z≈4m) were chosen. Although these depths at first inspection seem to be too conservative, they were chosen to reduce errors induced from the water/frame interaction around MISO and surface effects at the air/sea interface.

The meteorological station mounted on a 10 m tower in the sand dunes also collected data frequently, but the data was averaged down to two-minute time intervals prior to storage.

Data Orientation

Because the BADCP data was originally referenced to an Earth coordinate system, it was necessary to resolve the data into a cross-shore normal coordinate system. Upon installation, it was determined that the MISO frame had a referenced magnetic heading of 313° M. Using the center of the NPS lake as a reference, the direction to the MISO platform was ascertained to have a magnetic heading of 320° M. Therefore, to convert to a cross-shore normal coordinate system, the reference heading was subtracted from the magnetic heading (320° M - 313° M = 007° M). This 007° M conversion factor was then used in the data retrieval process to produce the two horizontal velocity vectors u and v. The u component represented the alongshore (AS) component while v represented the cross-shore (CS) component (Figure 4). The meteorological data was referenced to the cross-shore normal system prior to storage.

Data Preparation and Processing

Before employing any spectral analyses, it was necessary to manipulate the data set to (1) remove large errors, (2) ensure uniform temporal spacing, and (3) remove any gaps.

A major concern in processing ADCP data from the MISO data set was distinguishing the true current velocities from measurement errors or other erroneous values. Errors not representative of true current velocities occurred in the MISO data as a result of poor beam correlation values or fish or seaweed passing in front of the transducers. These errors were first discovered upon visual inspection of the time-series in its entirety. Separate plots of alongshore (u) and cross-shore (v) velocity components quickly revealed erroneous values in the raw data. Error detection and removal in this

manner, however, would have been tedious and time consuming. Instead, these erroneous data points were identified and removed in an automated deglitching routine consisting of a "de-spiking" routine. Great care was taken to make the data set as self-consistent as possible by establishing a conservative threshold level that would not reject important data points. Using an automated technique, any velocity data exceeding $\pm 3\sigma$ and not extending for more than five time intervals ($\approx$5 seconds) was replaced with interpolated values using a linear interpolation scheme.

After deglitching the current velocity data, both wind and current data sets were reduced to similar temporal spacing. Because the current velocity data was measured in seconds and the wind data had a sampling rate of two minutes, the BADCP data was averaged to two-minute time intervals. A one-minute window around each two-minute time interval was used for averaging to remove any errors induced from end effects.

With the knowledge that continuous (no gaps) meteorological observations began on April 28, 2000 (yearday 2000117), figure 5 was scrutinized to locate a suitable region for analysis where the BADCP had not failed for the majority of the time-series. In the end, a period of 100 days (yearday 2000175 to 2000275, or June 23-October 1, 2000) was selected for study. During this time period, there were only five short gaps (Figure 6).

In the last phase of the data preparation procedure, all of the gaps within the 100 day time-series were replaced with the overall mean current value. This step was necessary to conduct rotary cross-spectral estimates on the data. Prior to implementing the spectral analysis, however, the data sets are detrended using a linear scheme. Thus, there is little overall effect on the output by replacing the gaps with the mean.

Rotary Cross-Spectral Analysis

In order to characterize the degree of coupling between wind and surface / bottom current measurements, a statistical measure of the coherence and phase versus frequency as well as the power spectral density versus frequency was required. Normally, applying a cross-spectral analysis to the two time series (four Cartesian velocity vectors) would yield four phases and four correlation coefficients, thus making it difficult to ascertain if the time series were significantly coherent. In addition, the coherences would vary under coordinate rotation (i.e. the coherences would be dependent upon the orientation of the coordinate system in which the observations were made). More importantly however, rotary cross-spectral analysis allows the comparison of motion from vector quantities instead of scalar quantities.

To simplify the coherence analysis process and correct for these deficiencies, the four Cartesian velocity vectors were expressed as two complex-valued quantities of the form: $w_x = u_x + iv_x$. These complex velocity vectors were then decomposed for each frequency into two counter-rotating circular motions. These circularly polarized components (each with its own amplitude and phase) were later used to produce two-sided spectra where positive frequencies (f>0) corresponded to anticlockwise motion, and negative frequencies (f<0) corresponded to clockwise rotation. Inner and outer cross-spectral functions described the co-rotating and counter-rotating components, respectively. The following complex rotary cross-spectral methodology (as derived in Mooers, 1973 and simplified in Emery, 1997) was applied to the wind / near-surface current vectors and the wind / near-bottom current vectors shown in figures 7 and 8.

As an example, consider two vector time series (current velocity (c) and wind velocity (w)) defined by:

$$\begin{aligned} w_c &= u_c + iv_c \\ w_w &= u_w + iv_w \end{aligned} \tag{1}$$

respectively. Taking the Fourier transform of both the current and wind complex time series yields:

$$W(f) = \begin{cases} A^+ e^{(-i\theta^+)}, f \geq 0 \\ A^- e^{(-i\theta^-)}, f \leq 0 \end{cases} \tag{2}$$

Equation 2 associates the negative frequencies with the clockwise rotary components and the positive Fourier transform frequencies with the anticlockwise rotary components.

Inner cross-spectrum: The inner cross-spectrum $S_{cw}(f)$ compares the joint energy of the current and wind time series for the rotary components rotating in the same direction (e.g. the clockwise component of the wind vector to the clockwise component of the near-surface current vector)

$$\begin{aligned} S_{cw}(f) &= \left\langle W_c^*(f) W_w(f) \right\rangle \\ &= \begin{cases} A_c^+(f) A_w^+(f) e^{[-i(\theta_c^+ - \theta_w^+)]}, f \geq 0 \\ A_c^-(f) A_w^-(f) e^{[-i(\theta_c^- - \theta_w^-)]}, f \leq 0 \end{cases} \end{aligned} \tag{3}$$

with * denoting the complex conjugate and $\langle \bullet \rangle$ representing an ensemble average.

Inner autospectrum: The autospectrum for each time series is then:

$$S_{cc} = \begin{cases} [A_c^+(f)]^2, f \geq 0 \\ [A_c^-(f)]^2, f \leq 0 \end{cases} \quad (4)$$

$$S_{ww} = \begin{cases} [A_w^+(f)]^2, f \geq 0 \\ [A_w^-(f)]^2, f \leq 0 \end{cases} \quad (5)$$

Thus, as an example, S_{cc} ($f \geq 0$) is the power spectral density of the anticlockwise component of the current time-series. The area under this curve versus frequency will therefore equal the variance of the cross-shore and along-shore current velocity components.

Inner coherence squared: The inner coherence-squared between the wind and current time series at frequency (*f*) is calculated according to:

$$C_{cw} = \begin{cases} \left\{ \left\langle A_1^+ A_2^+ \cos(\theta_1^+ - \theta_2^+) \right\rangle^2 + \left\langle A_1^+ A_2^+ \sin(\theta_1^+ - \theta_2^+) \right\rangle^2 \right\} / \left\langle A_1^{+2} \right\rangle \left\langle A_2^{+2} \right\rangle, f \geq 0 \\ \left\{ \left\langle A_1^- A_2^- \cos(\theta_1^- - \theta_2^-) \right\rangle^2 + \left\langle A_1^- A_2^- \sin(\theta_1^- - \theta_2^-) \right\rangle^2 \right\} / \left\langle A_1^{-2} \right\rangle \left\langle A_2^{-2} \right\rangle, f \leq 0 \end{cases} \quad (6)$$

The coherence C_{cw} ranges from 0 to 1, and represents the similarity (or variability) of the two time series to each other. A value near unity indicates a high degree of correlation, while a coherence near zero indicates a negligible correlation. Using a 95% confidence interval, equation 7 provides a limiting value, or level to which coherence-squared values occur by chance:

$$C_{cw}^{significant} = 1 - 0.5^{[2/(DOF-2)]} \quad (7)$$

where DOF represents the degrees of freedom contained in the time-series.

Inner phase: The phase for the cross spectrum and coherence measures the phase lead of the rotary component of the current time-series with respect to the wind time-series. It can be calculated according to the following equation:

$$\tan(\phi_{cw}) = \begin{cases} \left\{ \left\langle A_c^+ A_w^+ \sin(\theta_c^+ - \theta_w^+) \right\rangle^2 / \left\langle A_c^+ A_w^+ \cos(\theta_c^+ - \theta_w^+) \right\rangle^2 \right\}, f \geq 0 \\ \left\{ \left\langle -A_c^- A_w^- \sin(\theta_c^- - \theta_w^-) \right\rangle^2 / \left\langle A_c^- A_w^- \cos(\theta_c^- - \theta_w^-) \right\rangle^2 \right\}, f \leq 0 \end{cases} \quad (8)$$

Outer cross-spectrum: The outer cross-spectrum $O_{cw}(f)$ compares the joint energy of the current and wind time series for the rotary components rotating in the <u>opposite</u> direction (e.g. the clockwise component of the wind vector to the anticlockwise component of the near-surface current vector).

$$\begin{aligned} O_{cw}(f) &= \left\langle W_c(-f) W_w(f) \right\rangle \\ &= \begin{cases} A_c^-(f) A_w^+(f) e^{[i(\theta_c^+ - \theta_w^-)]}, f \geq 0 \\ A_c^+(f) A_w^-(f) e^{[i(\theta_c^+ - \theta_w^+)]}, f \leq 0 \end{cases} \end{aligned} \quad (9)$$

Outer autospectrum: The outer rotary autospectrum for each time series is then:

$$O_{cc} = A_c^-(f) A_c^+(f) e^{[i(\theta_c^+ - \theta_c^-)]}, f \geq 0 \quad (10)$$

$$O_{ww} = A_w^-(f) A_w^+(f) e^{[i(\theta_w^+ - \theta_w^-)]}, f \geq 0 \quad (11)$$

Both outer power spectral densities are symmetric about f=0.

Outer coherence squared: The outer coherence squared between the wind and current time series at frequency (*f*) is calculated according to:

$$D_{cw} = \begin{cases} \left\langle A_c^- A_w^+ \right\rangle \left[\left\langle \cos(\theta_w^+ - \theta_c^-) \right\rangle^2 + \left\langle \sin(\theta_w^+ - \theta_c^+) \right\rangle^2 \right] / \left\langle A_w^{+2} \right\rangle \left\langle A_c^{-2} \right\rangle, f \geq 0 \\ \left\langle A_c^+ A_w^- \right\rangle \left[\left\langle \cos(\theta_c^+ - \theta_w^-) \right\rangle^2 + \left\langle \sin(\theta_c^+ - \theta_w^+) \right\rangle^2 \right] / \left\langle A_c^{+2} \right\rangle \left\langle A_w^{-2} \right\rangle, f \leq 0 \end{cases} \quad (12)$$

Outer phase: The phase for the outer cross-spectrum and coherence is given by:

$$\tan(\psi_{cw}) = \begin{cases} \left\{ \left\langle A_c^- A_w^+ \sin(\theta_c^- - \theta_w^+) \right\rangle / \left\langle A_c^- A_w^+ \cos(\theta_c^- - \theta_w^+) \right\rangle \right\}, f \geq 0 \\ \left\{ \left\langle A_c^+ A_w^- \sin(\theta_c^- - \theta_w^+) \right\rangle / \left\langle A_c^+ A_w^- \cos(\theta_c^- - \theta_w^-) \right\rangle \right\}, f \leq 0 \end{cases} \quad (13)$$

Example Calculations

In order to better illustrate the execution of this methodology, two counter-rotating circular sinusoidal waves of equal magnitude were generated with superimposed noise (Figure 9). Appendix A contains the formulae for executing this test. After the complex rotary cross-spectral analysis was conducted, the inner autospectra of each component (Figure 10) and the inner cross-spectral density (Figure 11) were plotted versus frequency. Figure 10 clearly shows that all of the energy in the first signal (designed for anticlockwise rotation) does indeed reside in the positive frequency realm. Likewise, all of the energy in the second signal (clockwise rotation) can be found in the negative frequency range. The outer cross-spectral energy plot in figure 11 shows that both the clockwise and anticlockwise energy are equal in magnitude, as expected from the original wave design.

RESULTS AND DISCUSSION

After all of the processing was complete, each parameter of the inner rotary analysis was plotted versus frequency. The outer rotary spectra output was largely unused as determining the coupling of oppositely rotating components was not within the scope of this project.

The inner near-surface power spectral density (Figure 12) shows the possibility of coupling between the wind (anticlockwise) and the diurnal near-surface current (clockwise) rotary autospectra components. Interestingly, the semi-diurnal near-surface current (anti-clockwise) and the wind (clockwise) also show the possibility of coupling as evidenced by the coincidental energy peaks. The coherence levels (Figure 13) are significant (with a 95% confidence level) at the diurnal peak, and the near-surface current leads the wind signal by a phase of 90°.

Like the near-surface PSD, the inner near-bottom power spectral density (Figure 14) shows similar energy peaks between opposite rotary components at both the diurnal and semi-diurnal frequencies. Upon comparison to the near-surface peak magnitudes, however, the near-bottom condition contains less energy. The coherences for the near-bottom case are less significant, and the phase angles are inconsistent (Figure 15).

Figure 16 depicts the inner cross-spectral energy of the near-surface and near-bottom conditions as compared to the wind. For the near-surface case, the clockwise current / wind cross-spectrum energy is greater than the anti-clockwise component. The near-bottom case, however, shows an increase in diurnal anticlockwise energy, and a slight decrease in the diurnal clockwise direction.

From the above results, it can be concluded that surface and bottom coupling between the wind and the horizontal currents could exist. The decrease in energy between the surface and the bottom currents could indicate a deep log layer in unstratified (well-mixed) conditions, or the presence of stratification with a slippery surface layer. Upon inspection of the coherence levels, however, one can conclude that the near-surface current and wind velocities are coupled, while the near-bottom current and wind velocities frequently are frequently decoupled over the 100 day time-series. The surface phase angles around 90° reflect Eckman coupling at the surface boundary layer, though the limited time-series results in a large phase error. The bottom phase relationship are not robust due to the reduced coherence, reflecting de-coupling of bottom current with the wind.

BIBLIOGRAPHY

Emery, W.J. and R.E. Thomson. 1997: Data analysis methods in physical oceanography. Gray Publishing, Kentucky.

Gonella, J. 1972: A rotary component method for analyzing meteorological and oceanographic vector time series. *Deep-Sea Res., 19*, 833-846.

Middleton, J.H. 1982: Outer rotary cross spectra, coherences and phases. *Deep-Sea Res., 29(10A),* 1267-1269.

Mooers, C.N.K. 1973: A technique for the cross spectrum analysis of pairs of complex-valued time series, with emphasis on properties of polarized components and rotational invariants. *Deep-Sea Res., 20*, 1129-1141.

Press, W.H., et al. 1986: Numerical recipes, the art of scientific computing. Cambridge University Press, NY.

Figure 1. Location of the MISO instrument platform. The star represents the location of the MISO array.

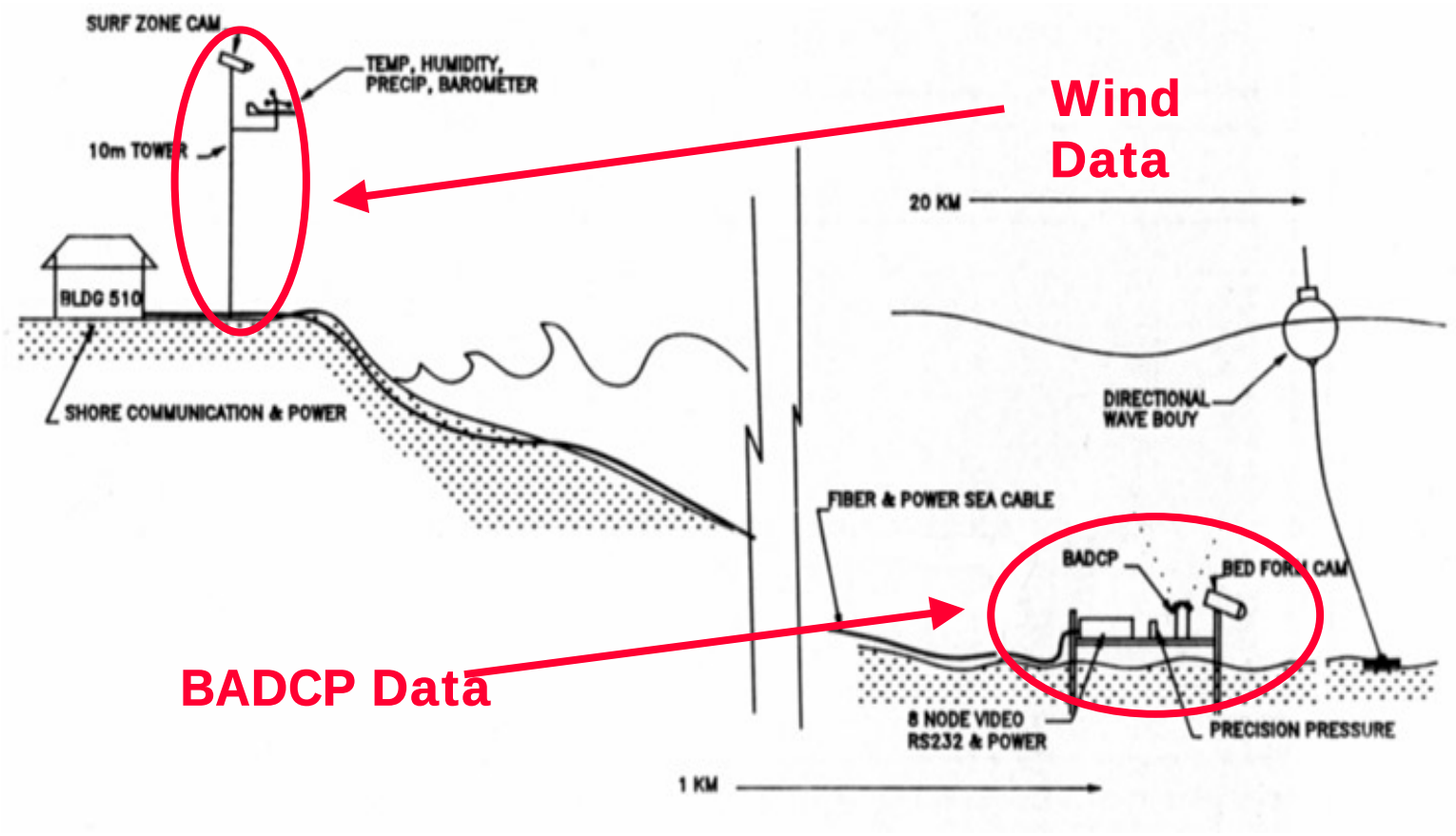

Figure 2. MISO frame and meteorological configuration.

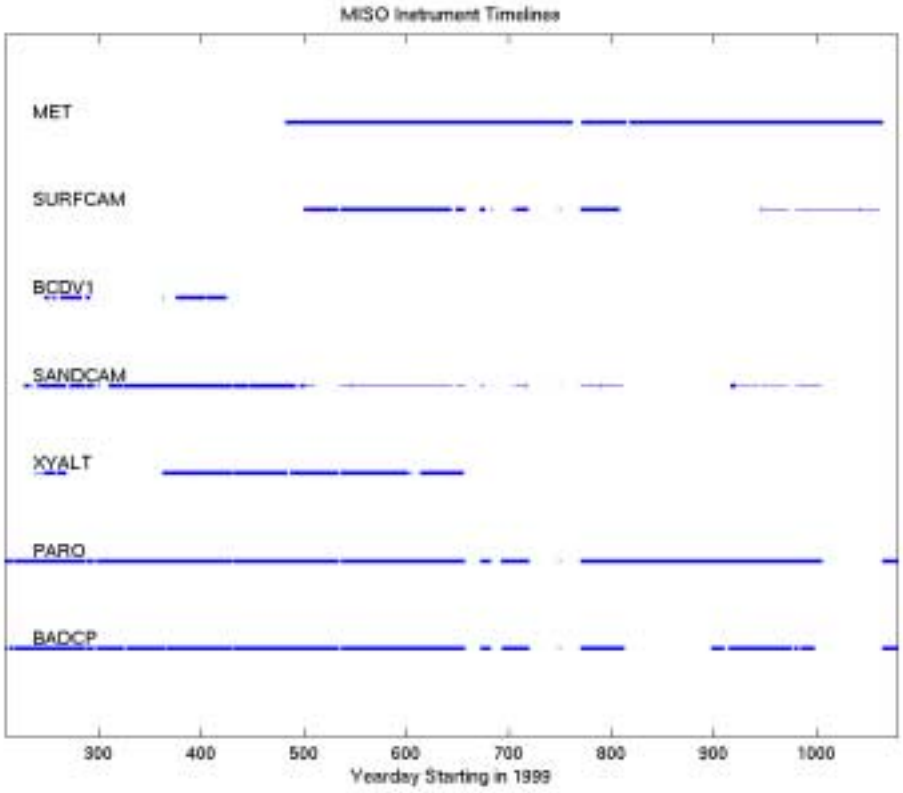

Figure 3. MISO instrument timeline. MISO started collecting data on July 26, 1999 while the meteorological station (denoted MET) began on April 28, 2000. The above timeline indicates when each instrument mounted on the MISO frame collected data. Gaps indicate instrument failure, malfunction, or maintenance.

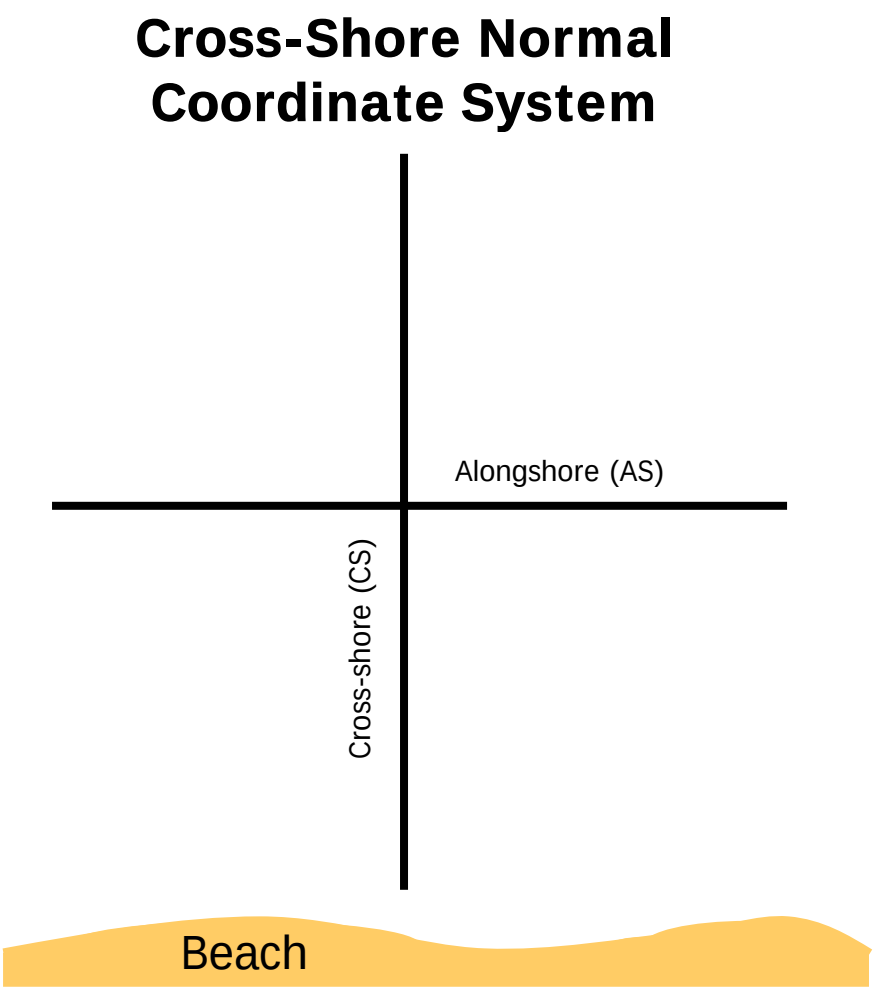

Figure 4. Cross-Shore Normal Coordinate System off Del Monte Beach in Monterey Bay, CA.

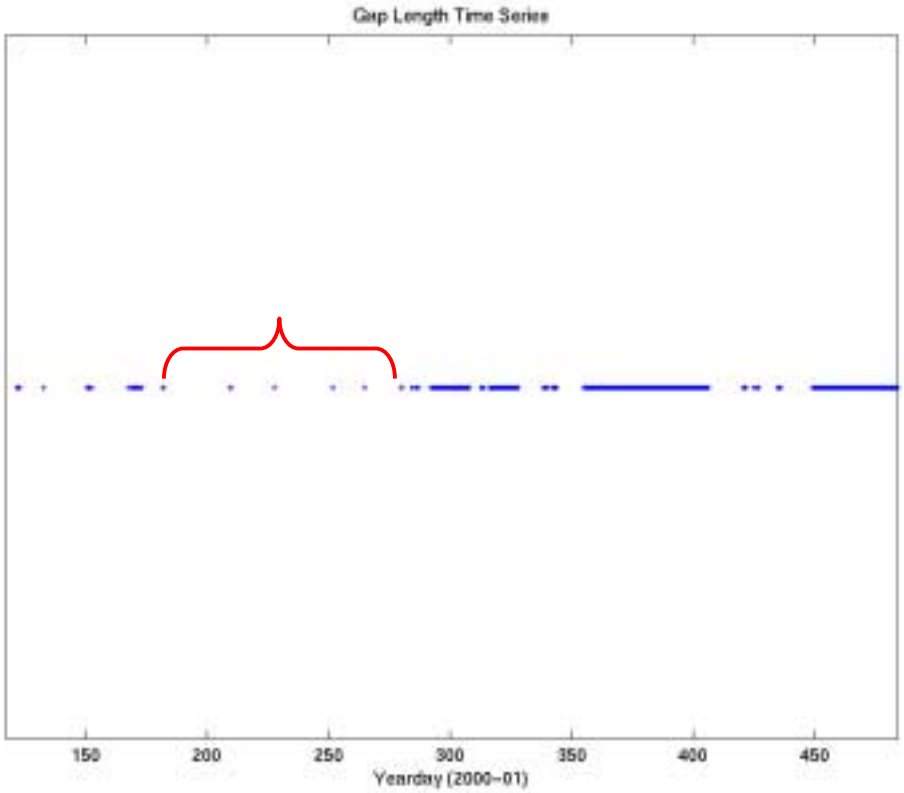

Figure 5. Timeline of gaps in BADCP time-series. The bracket indicates the portion of the time-series selected for this study. Note: only five small gaps occurred during this time.

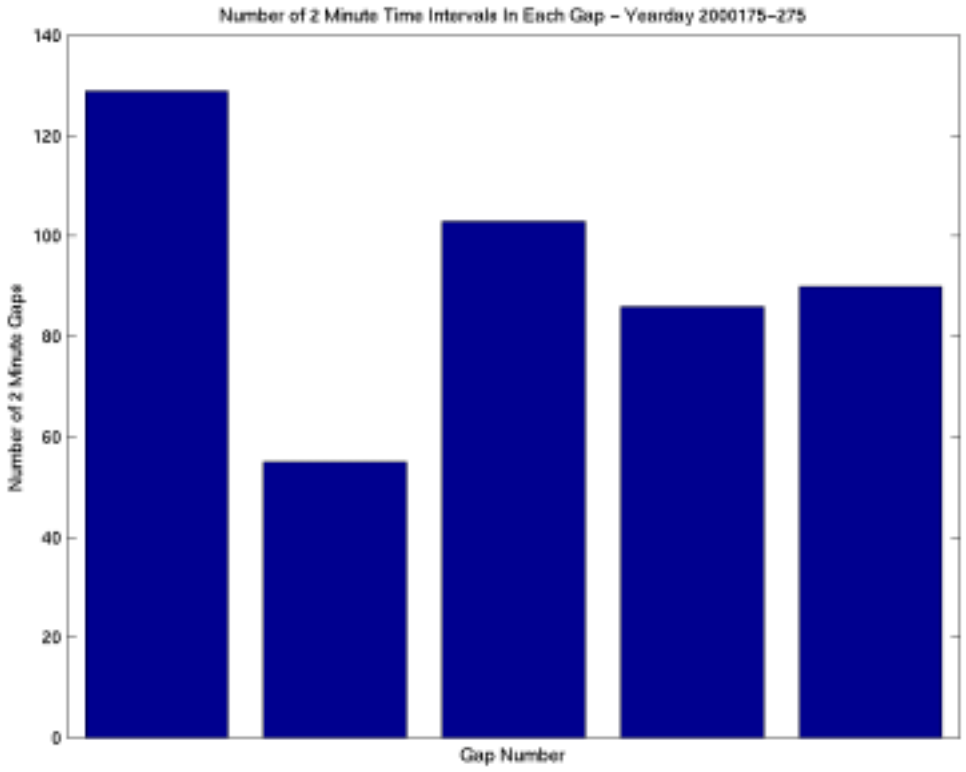

Figure 6. Gap length of time-series.

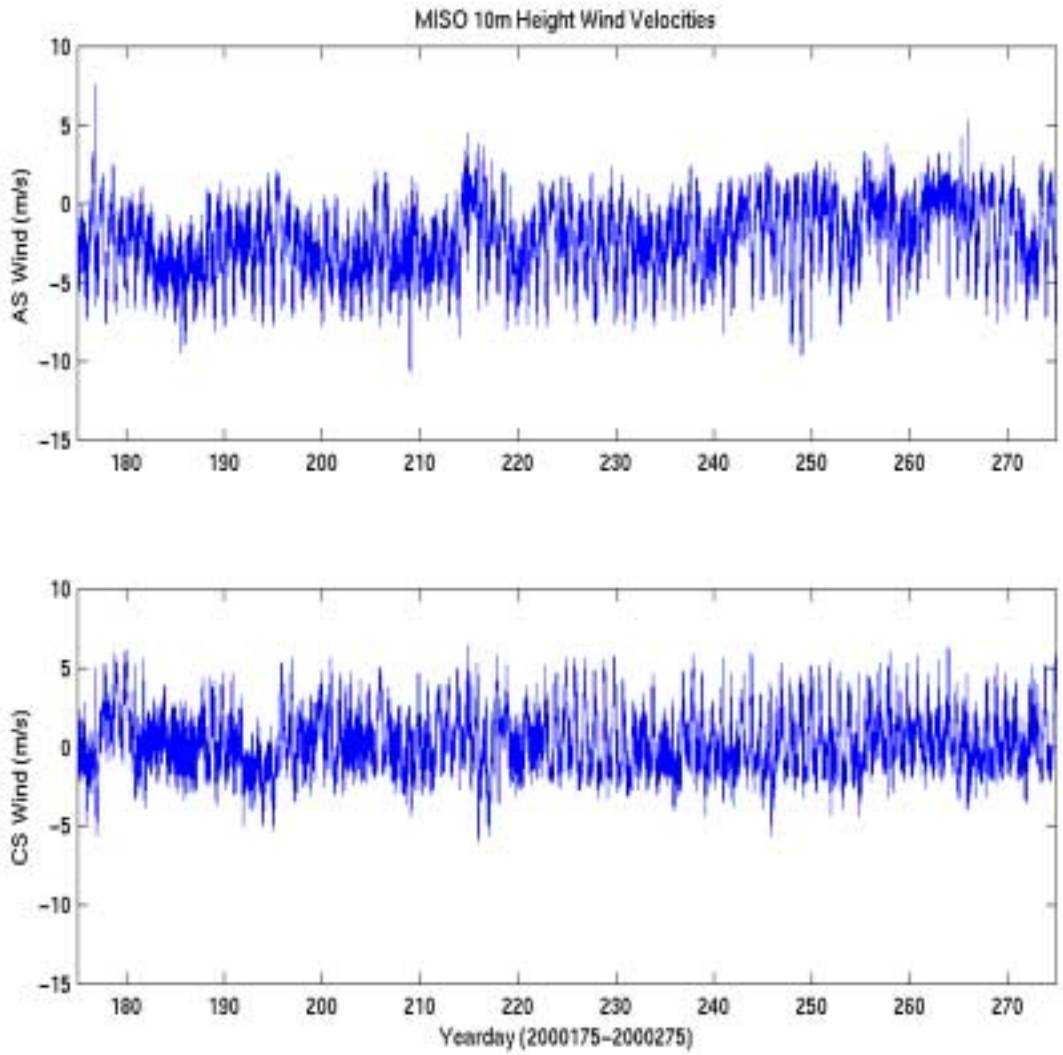

Figure 7. Wind time-series for yearday 2000175-2000275.

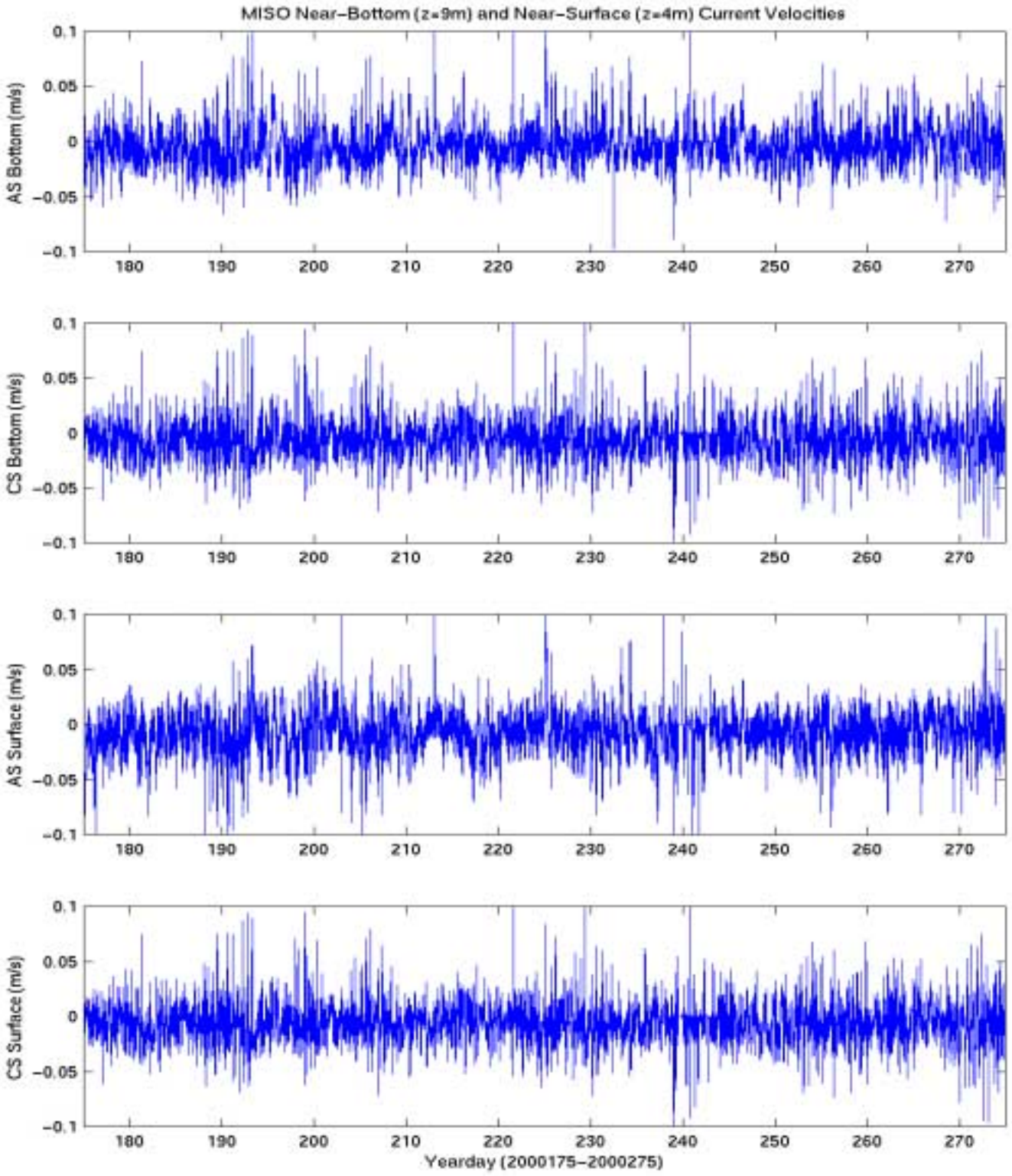

Figure 8. Horizontal current time-series for yearday 2000175-2000275.

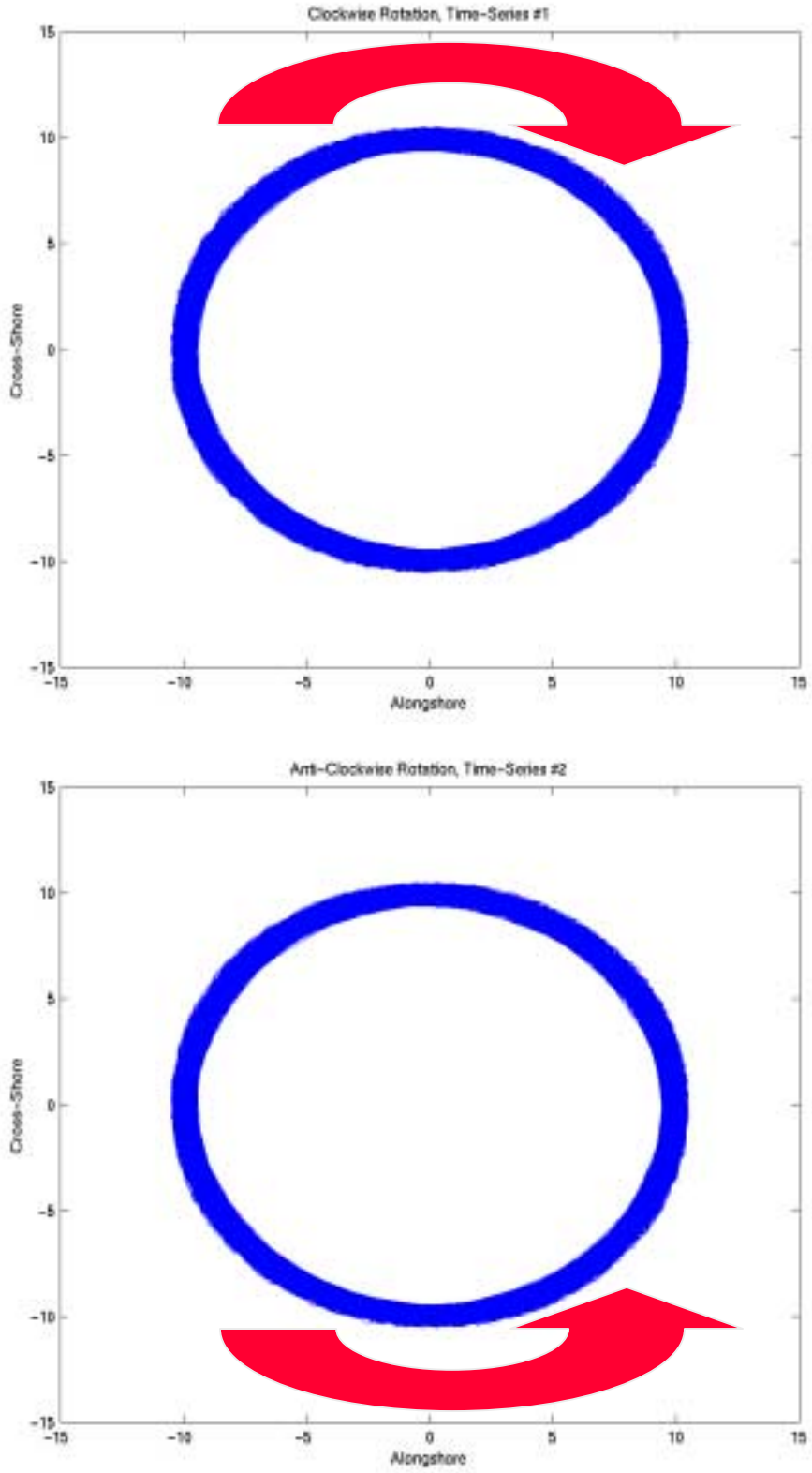

Figure 9. Two randomly generated counter-rotating circular sinusoidal waves of equal magnitude.

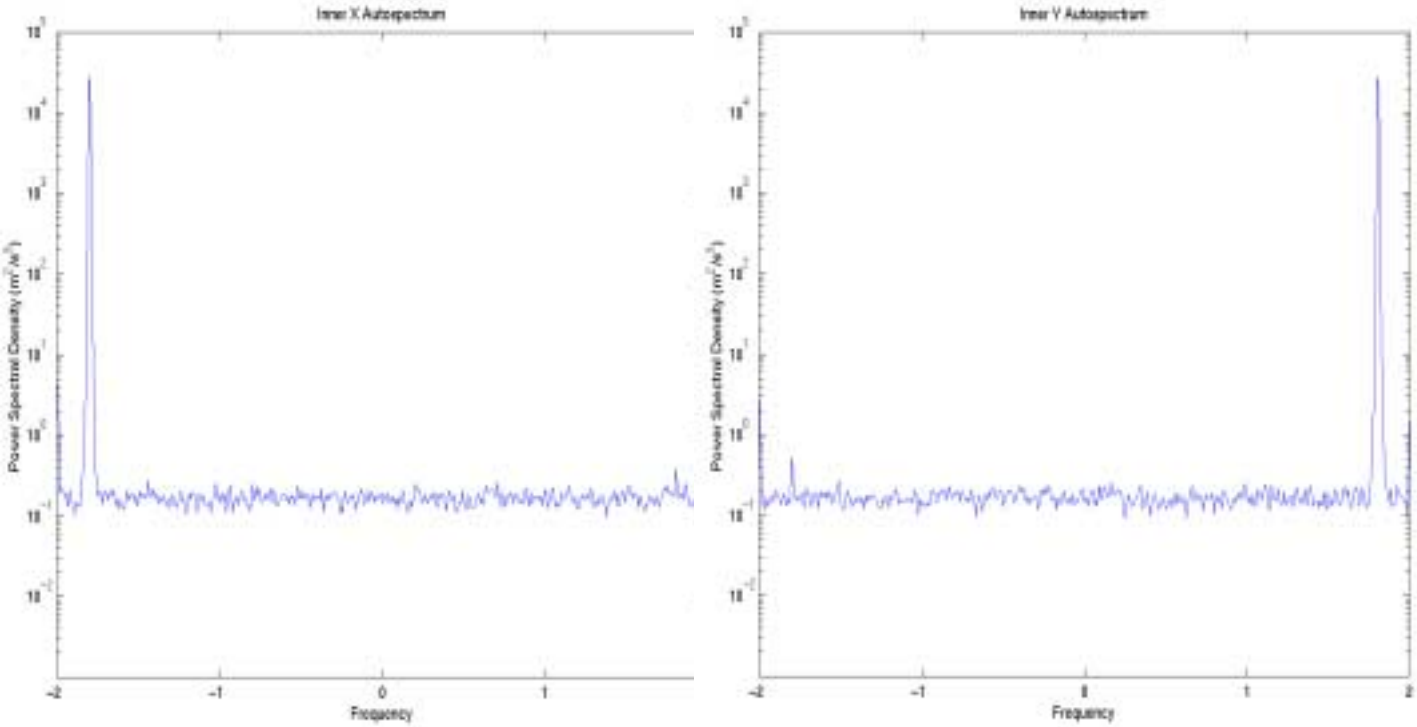

Figure 10. Inner autospectra output from rotary analysis of randomly generated circular waves.

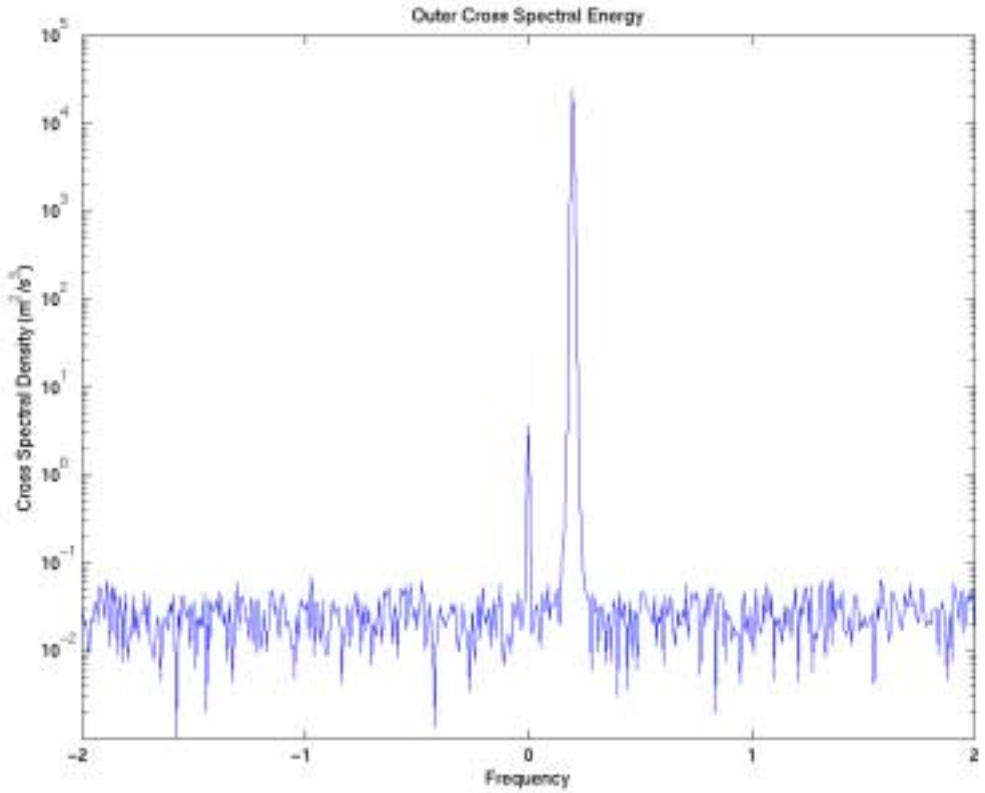

Figure 11. Outer cross spectrum output from rotary analysis of randomly generated circular waves.

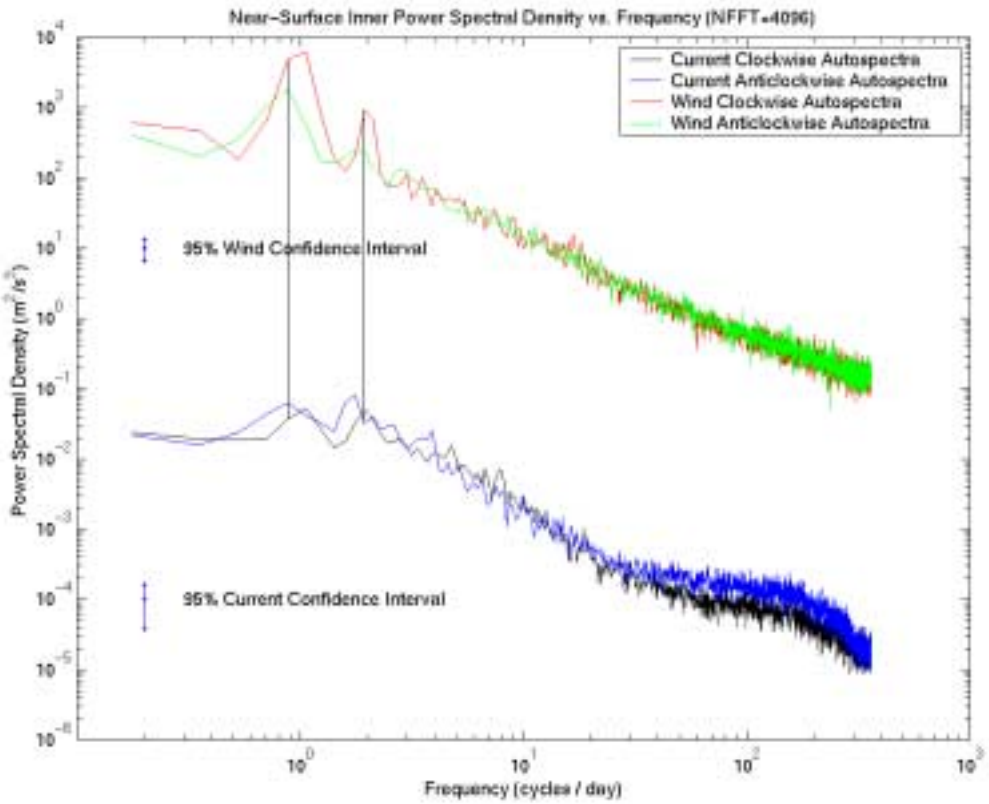

Figure 12. Near-surface inner power spectral densities of both rotary components of wind and current time-series.

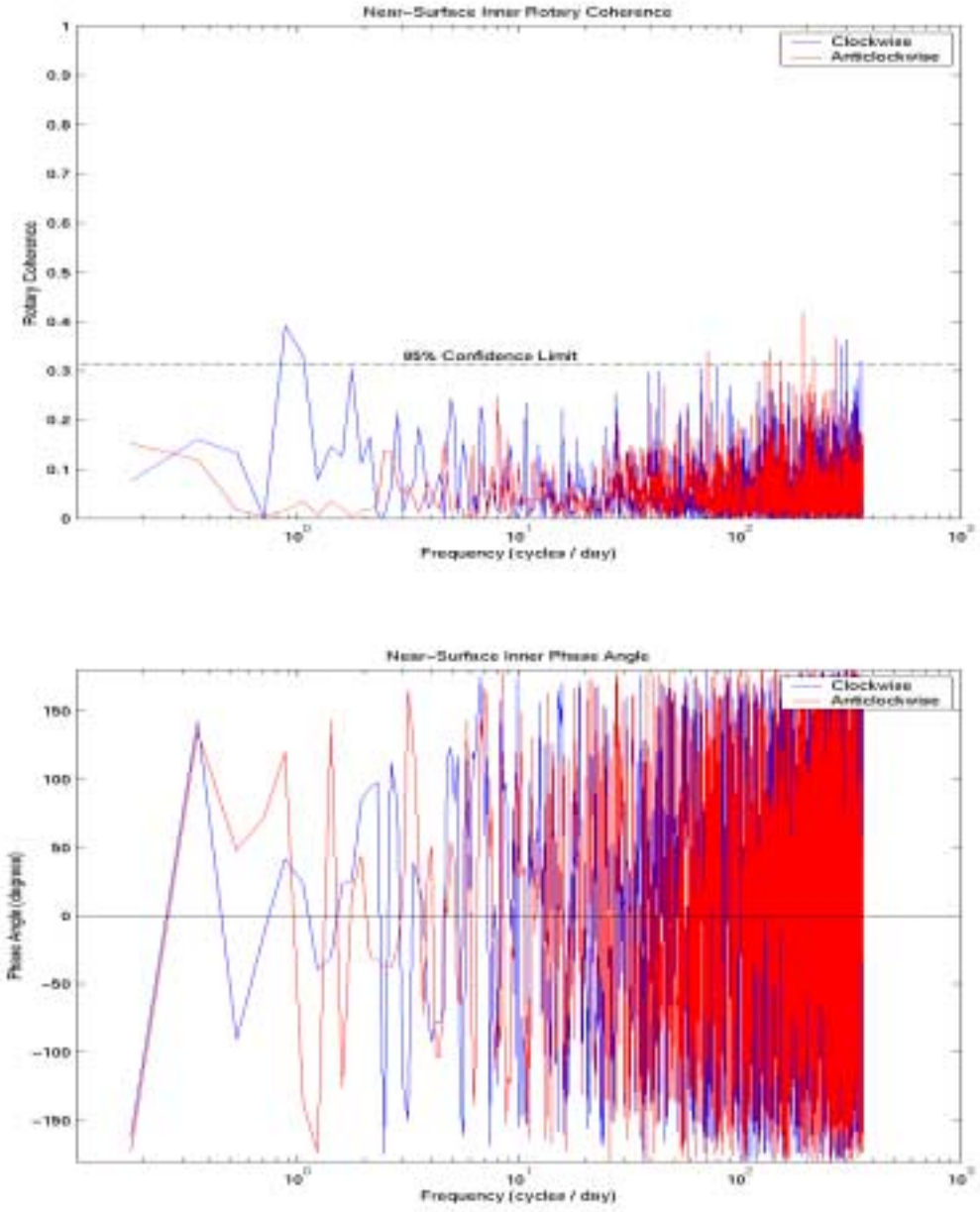

Figure 13. Near-surface inner coherence (top) and phase angle (bottom).

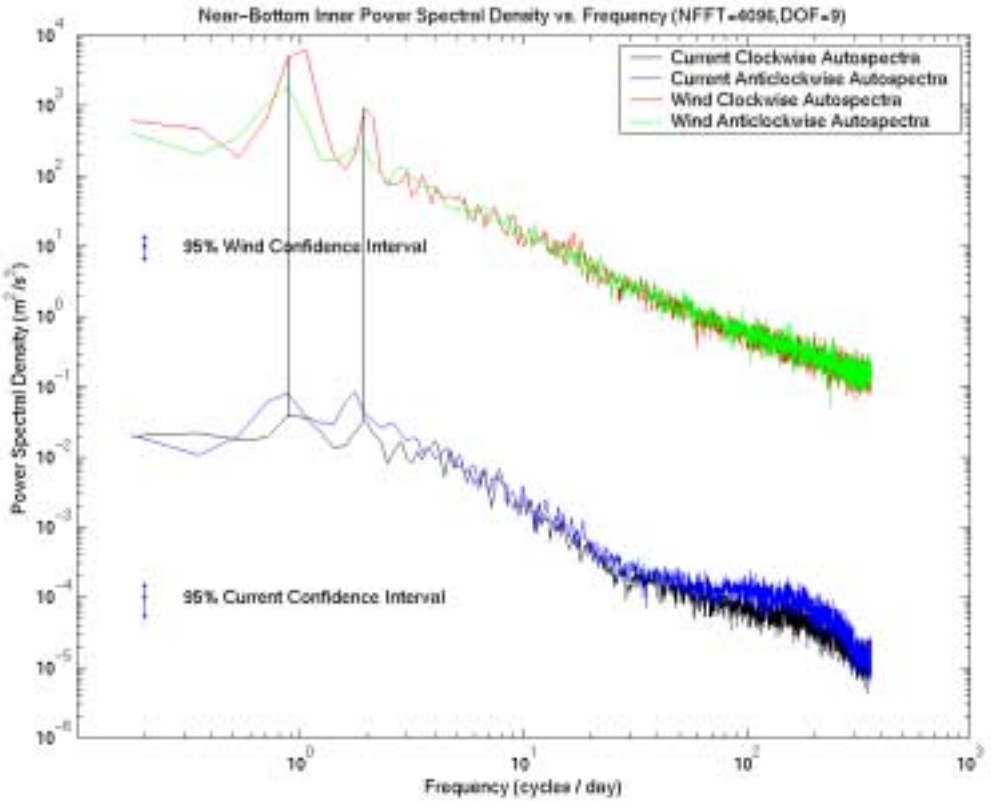

Figure 14. Near-bottom inner power spectral densities of both rotary components of wind and current time-series.

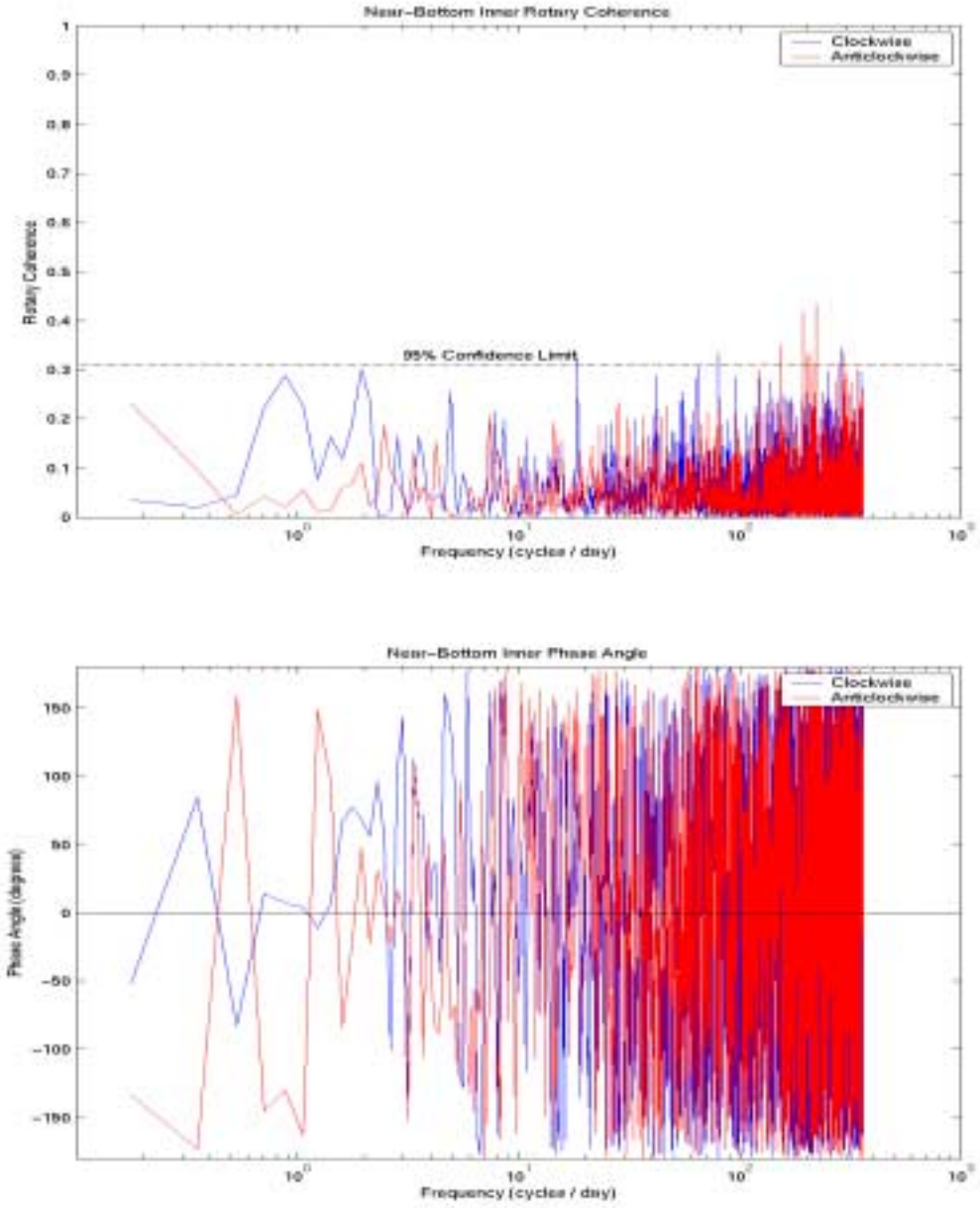

Figure 15. Near-bottom inner coherence (top) and phase angle (bottom).

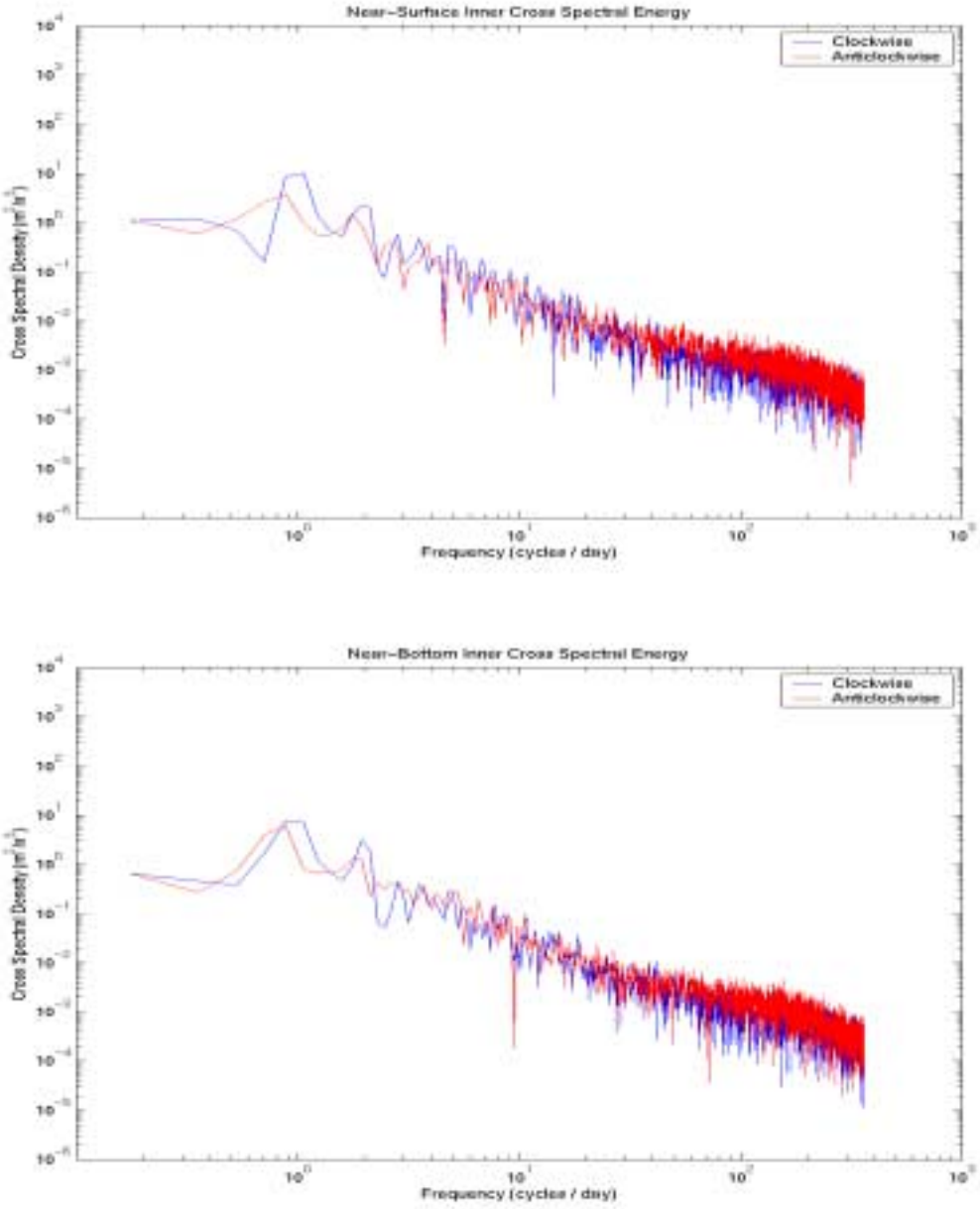

Figure 16. Near-surface and near-bottom inner cross-spectral densities of both rotary components.